The Superposition of Eastward and Westward Rossby Waves in Response to Localized Forcing

Citation

Shaman, Jeffrey, and Eli Tziperman. 2016. "The Superposition of Eastward and Westward Rossby Waves in Response to Localized Forcing." Journal of Climate 29 (20): 7547–57. https://doi.org/10.1175/jcli-d-16-0119.1.

Permanent link

http://nrs.harvard.edu/urn-3:HUL.InstRepos:41384991

Terms of Use

Share Your Story

The Harvard community has made this article openly available.
Please share how this access benefits you. Submit a story .

Accessibility

The Superposition of Eastward and Westward Rossby Waves in Response to Localized Forcing

JEFFREY SHAMAN

Department of Environmental Health Sciences, Columbia University, New York, New York

ELI TZIPERMAN

Department of Earth and Planetary Sciences, and School of Engineering and Applied Sciences, Harvard University, Cambridge, Massachusetts

ABSTRACT

Rossby waves are a principal form of atmospheric communication between disparate parts of the climate system. These planetary waves are typically excited by diabatic or orographic forcing and can be subject to considerable downstream modification. Because of differences in wave properties, including vertical structure, phase speed, and group velocity, Rossby waves exhibit a wide range of behaviors. This study demonstrates the combined effects of eastward-propagating stationary barotropic Rossby waves and westward-propagating very-low-zonal-wavenumber stationary barotropic Rossby waves on the atmospheric response to wintertime El Niño convective forcing over the tropical Pacific. Experiments are conducted using the Community Atmosphere Model, version 4.0, in which both diabatic forcing over the Pacific and localized relaxation outside the forcing region are applied. The localized relaxation is used to dampen Rossby wave propagation to either the west or east of the forcing region and isolate the alternate direction signal. The experiments reveal that El Niño forcing produces both eastward- and westward-propagating stationary waves in the upper troposphere. Over North Africa and Asia the aggregate undamped upper-tropospheric response is due to the superposition and interaction of these oppositely directed planetary waves that emanate from the forcing region and encircle the planet.

1. Introduction

Studies of atmospheric planetary wave dynamics date back to their first description by Carl-Gustav Rossby (e.g., Rossby 1939). These waves are responsible for a substantial portion of the large-scale communication, or teleconnection, of remotely forced variability around the planet. Synoptic variability, jet stream meanderings, and large-scale climate patterns [e.g., the Pacific–North American (PNA) pattern] have all been described in the context of Rossby waves. In particular, studies of stationary planetary waves—waves for which the wave movement and background flow balance so that the phase speed is zero—have been used to explain a number of physical phenomena, including remote changes in pressure, wind, and precipitation patterns due to thermal and orographic forcing (Hoskins and Karoly 1981), interactions within the extratropics (Wang et al. 2007), equatorial Rossby waves (Sobel and Bretherton 1999; Kucharski et al. 2009), and tropical–extratropical interactions (Hoskins and Karoly 1981). In addition, other studies have explored the Rossby wave response to low-frequency forcing (Li and Nathan 1997), as well as the activity of Rossby waves with very small (Shaman et al. 2009) and complex wavenumbers (Shaman et al. 2012). In aggregate, these studies indicate there exists a variety of Rossby waveforms with a multeity of impacts on the atmosphere.

Rossby wave behavior can be studied from a theoretical vantage, as well as by using simple models and analytic techniques. The latter approaches, which employ tools such as vorticity equation models or ray tracing, isolate the effects of Rossby waves to the exclusion of all other processes.

Corresponding author address: Jeffrey Shaman, Department of Environmental Health Sciences, Mailman School of Public Health, Columbia University, 722 West 168th Street, Rosenfield Building, Room 1104C, New York, NY 10032.
E-mail: jls106@columbia.edu

In contrast, general circulation models (GCMs) allow study of the full range of dynamics, thermodynamics, and radiative processes that affect the atmosphere. Indeed, these models contain the full spectrum of Rossby waves, as well as other processes. In this richer, more complex environment, it is sometimes difficult to identify the role of individual wave processes and propagation mechanisms from the combined signal owing to the superposition and interaction of waves.

Here we implement a sponge relaxation scheme designed to dampen wave propagation in a selected direction in the Community Atmosphere Model, version 4.0 (CAM4.0). We first demonstrate the effectiveness of the relaxation damping scheme and then use it in conjunction with diabatic forcing over the tropical Pacific to study how remote influences are effected through the superposition and interaction of eastward- and westward-propagating Rossby waves initiated in response to a single forcing. Specifically, we focus on tropical-to-extratropical wave activity in response to El Niño–related forcing in the North African–Asian (NAA) jet over the Tibetan Plateau. Section 2 presents the model, sponge damping methodology, and experimental design. Section 3 reviews Rossby wave theory, including evidence for the existence of ultralow-wavenumber Rossby waves. Section 4 further demonstrates the effectiveness of the sponge and presents novel findings, and discussion is provided in section 5.

2. Methods

Simulations were performed using the CAM4.0 atmospheric general circulation model (AGCM) (Neale et al. 2010). Integrations were run at 1.9° × 2.5° resolution with 26 levels in the vertical. All simulations were performed using perpetual February settings forced with February monthly averaged climatological merged Hadley Centre Sea Ice and Sea Surface Temperature dataset (HadISST) and NOAA Optimum Interpolation Sea Surface Temperature (OISST) values of SSTs and sea ice concentrations (Hurrell et al. 2008) and 14 February orbital forcing. The model diurnal cycle was retained. As applied, the perpetual setting removes the seasonal cycle, the Northern Hemisphere remains colder than the Southern Hemisphere, synoptic variability is retained, and there is no secular trend indicative of longer-time-scale warming or cooling.

The model was first integrated for 55 years in this setting. The final 50 years of this simulation were then averaged to establish model baseline February climatological conditions. Climatological dry static energy and zonal and meridional winds were then extracted for use with the sponge relaxation scheme.

Most remaining simulations were performed with sponge relaxation, which was implemented in order to dampen wave propagation. This sponge relaxation was localized to particular regions of the model planet, either to the east or west of the forcing region, typically in a longitudinal band extending from pole to pole and through all vertical levels. The sponge was applied to dry static energy and horizontal winds at each updating of the CAM4.0 physics package, such that an updated, relaxed variable S_{sponge} is given by the following:

$$S_{sponge} = S_{state} + \frac{\Delta t}{\Gamma}(S_{clim} - S_{state}), \qquad (1)$$

where S_{state} is the current model state of variable S (either the dry static energy, zonal wind, or meridional wind field) at time t, Δt is the model time step, Γ is the imposed relaxation time scale of the sponge, and S_{clim} is the 50-yr climatological value of variable S. The Γ was imposed at 2.5 days. To minimize edge effects, to either side of the region of full-strength relaxation a 10° buffer was imposed in which the strength of relaxation decayed as a Gaussian function of distance. The sponge effectively restores dry static energy and wind conditions to their 50-yr climatology where applied (Fig. 1). Indeed eddy deviations from the time mean are near eliminated; consequently, waves, including midlatitude baroclinic wave activity, entering the sponge are damped and fail to propagate through the sponge region.

Simulations with the sponge were performed both with and without additional diabatic forcing. This diabatic forcing was imposed, per Barlow et al. (2007), during calculation of physical processes in the tphysbc. F90 subroutine of CAM4.0. For the experiments presented here, the forcing was designed to mimic the anomalous diabatic heating due to convection associated with February El Niño conditions. Specifically, diabatic heating was applied over 10°S–10°N, 160°–220°E and 0°–10°N, 220°–280°E, mirroring the spatial extent and orientation of precipitation anomalies associated with El Niño. The magnitude of the diabatic heating was applied as an idealized half-sine wave in both latitude and longitude. In the vertical, the forcing was applied between 780 and 220 hPa and had an approximate half-sine structure, skewed toward the upper troposphere, that maximized around 430 hPa at 0.04 J s^{-1}.

Experiments were performed to determine how sponge relaxation affects Rossby wave propagation and the overall atmospheric response in CAM4.0. The time-mean average of simulations with a particular sponge setting was subtracted from the time-mean average of simulations with the same sponge and El Niño diabatic forcing. This differencing indicates how the sponge alters wave propagation. By including the sponge in both the
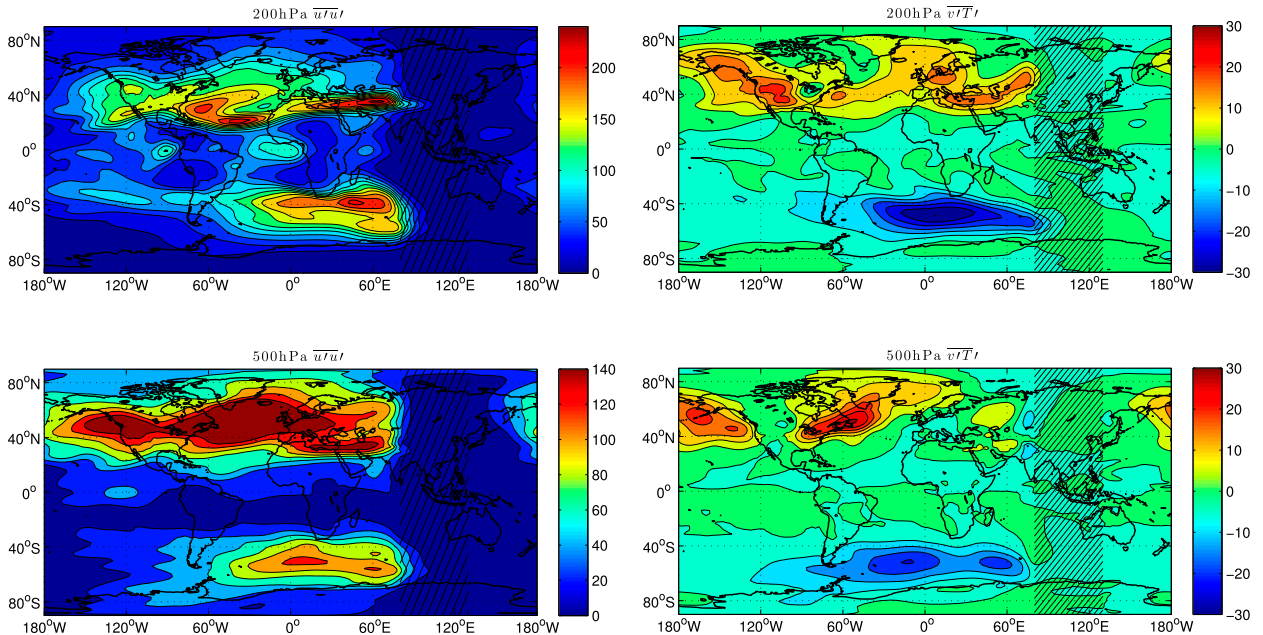
FIG. 1. (left) Average eddy zonal momentum flux ($\overline{u'u'} = \overline{uu} - \overline{u} \times \overline{u}$) for years 6–20 of an integration with sponge damping applied from 80° to 130°E (shown by the hatched region). The damping effectively eliminates eddy flux signal within the sponge region. The sponge also effectively damps baroclinic wave activity. The contour interval is $20\,\mathrm{m^2\,s^{-2}}$. (right) Average eddy meridional heat flux ($\overline{v'T'} = \overline{vT} - \overline{v} \times \overline{T}$) for years 6–20 of an integration with sponge damping applied from 80° to 130°E (shown by the hatched region). Overbars represent the climatological mean and primes the deviation from that mean. The contour interval is $10\,\mathrm{m\,K\,s^{-1}}$.

forced and unforced runs, we controlled for any wave activity generated by the sponge itself. Control runs, with no sponge, were also performed both with and without El Niño diabatic forcing.

Including a 5-yr window to allow for model spinup, simulations were conducted for periods of 10, 20, and 55 years. Results were similar for these different run lengths, so here we present the results from the final 15 years (years 6–20) of the 20-yr integrations.

3. Review of eastward and westward Rossby wave teleconnection mechanisms

Large-scale tropical-to-extratropical atmospheric communication is typically characterized and understood as the consequence of planetary wave activity. Specifically, thermal forcing in the tropics excites poleward- and eastward-propagating stationary barotropic Rossby waves (Hoskins and Karoly 1981), which produce anomalous standing patterns that persist, depending on the time scale of the forcing, from weeks to seasons. The waves themselves can be subject to considerable modification downstream of the forcing region due to synoptic-scale transients (Held et al. 1989; Trenberth et al. 1998), interaction with jet exit regions or other components of the climatological stationary wave field (Simmons et al. 1983; Branstator 1985; Hoerling and Ting 1994; Shaman 2014),

subtropical convergence associated with the initial thermal forcing (Held and Kang 1987), and orographic effects (Nigam and DeWeaver 1998). These effects often reinforce the Rossby wave train signal.

To further describe this barotropic wave activity, consider the two-dimensional, approximate plane wave solution with slowly varying amplitude, wavenumber, and position of the form $A \exp[i\phi(x, y, t)]$, where A is the wave amplitude, i is the imaginary unit, x and y are zonal and meridional coordinates in Cartesian space, and ϕ is the wave phase, which can be expressed locally as follows:

$$\phi(x, y, t) \approx kx + ly - \omega t, \tag{2}$$

where $\omega(x, y, t) = -\partial\phi/\partial t$ is the slowly varying frequency, and $k(x, y, t) = \partial\phi/\partial x$ and $l(x, y, t) = \partial\phi/\partial y$ are slowly varying wavenumbers in the zonal and meridional directions, respectively. Per WKBJ theory, the length scale of the wave disturbance must be short—that is, there is rapid phase variation (Bender and Orszag 1978). The propagation of wave energy then moves along rays defined by

$$\frac{dx}{dt} = u_g = \frac{\partial\omega}{\partial k} \quad \text{and} \tag{3a}$$

$$\frac{dy}{dt} = v_g = \frac{\partial\omega}{\partial l}, \tag{3b}$$

where $\mathbf{c}_g = (u_g, v_g)$ is the group velocity vector, indicating the direction of wave energy propagation, and $d/dt = \partial/\partial t + \mathbf{c}_g \cdot \nabla$.

To determine this group velocity vector for a specific stationary wave type, the relevant dispersion relation is derived and solved for $\omega = 0$. Here we consider, per Karoly (1983), solutions to the nondivergent barotropic, quasigeostrophic vorticity equation linearized about a time-mean streamfunction climatology $\overline{\psi}(x, y)$ for a Mercator projection on a sphere. This perturbation streamfunction equation yields the following dispersion relation:

$$\omega(k, l, x, y) = \overline{u}_M k + \overline{v}_M l + \frac{l\partial\overline{q}/\partial x - k\partial\overline{q}/\partial y}{k^2 + l^2}, \quad (4)$$

where $(\overline{u}_M, \overline{v}_M) = (\overline{u}, \overline{v})/\cos\theta$ is the Mercator projection of the time-mean zonal and meridional winds, θ is latitude, $\overline{q} = 2\Omega\sin(\theta) + \nabla^2\overline{\psi}$ is the time-mean absolute vorticity, and Ω is the rotation rate of Earth.

Given Eq. (4), the group velocities for stationary barotropic Rossby waves resolve to

$$u_g = \overline{u}_M + \frac{(k^2 - l^2)\partial\overline{q}/\partial y - 2kl\partial\overline{q}/\partial x}{(k^2 + l^2)^2} \quad \text{and} \quad (5a)$$

$$v_g = \overline{v}_M + \frac{2kl\partial\overline{q}/\partial y + (k^2 - l^2)\partial\overline{q}/\partial x}{(k^2 + l^2)^2}. \quad (5b)$$

These group velocities indicate that two-dimensional Rossby waves can propagate in any direction. This behavior is in contrast to that derived for stationary barotropic Rossby waves in a zonally symmetric flow (see, e.g., Hoskins and Karoly 1981) for which Eq. (5a) reduces to $u_g = 2(\partial q/\partial y)k^2/(k^2 + l^2)^2$. This quantity is positive definite, indicative of eastward propagation, as $\partial q/\partial y$, the meridional gradient of absolute vorticity, is positive for eastward zonally symmetric flows.

The focus of the next sections is the propagation of stationary barotropic tropospheric Rossby waves in a realistic, zonally varying flow, for which Eqs. (5a) and (5b) are relevant. This two-dimensional form admits both positive and negative stationary wave group velocities and thus propagation in any direction—east, west, north, and south—depending on the background flow and wavenumbers.

In addition, Hoskins and Ambrizzi (1993) mentioned a special, long-zonal-wavelength form of westward-propagating stationary barotropic Rossby wave, which was further characterized in Shaman et al. (2009). This wave can be derived for either zonally symmetric or zonally varying time-mean flows. Specifically, as $k \to 0$, Eq. (5a) reduces to

$$u_g = \overline{u}_M - \frac{\partial\overline{q}/\partial y}{l^2}. \quad (6)$$

While their low wavenumber does violate the short wavelength assumptions of WKBJ theory, this description of these Rossby waves does seem to provide a framework for understanding and quantifying their behavior. In regions where $\overline{u}_M < (\partial\overline{q}/\partial y)/l^2$, this waveform propagates westward with a vorticity anomaly that appears single signed in the zonal direction owing to its long zonal wavelength. Such regions are often observed in jet streams, which support strong meridional gradients of vorticity. Indeed, experiments with a barotropic vorticity equation model linearized about reanalysis climatology revealed westward, single-signed vorticity anomaly propagation along a jet stream, upstream of the model forcing region. This anomalous vorticity signal translated with speeds matching those predicted by Eq. (6) (Shaman et al. 2009).

Figure 2 shows the quantities $\overline{u}_M - (\partial\overline{q}/\partial y)/l^2$, $\overline{u}_M$, and $\partial\overline{q}/\partial y$ for the 200-hPa level from a CAM4.0 simulation without forcing or sponge damping, using a Rossby wave with meridional half wavelength π/l of 3×10^6 m. The largest magnitudes of this quantity are seen in conjunction with the NAA jet, where zonal winds are strong and the meridional gradient of absolute vorticity is steep. Values are most negative just to the south of the NAA jet core with high positive values flanking this region along the jet periphery. The region of negative $\overline{u}_M - (\partial\overline{q}/\partial y)/l^2$ can support rapid westward propagation of low-zonal-wavenumber Rossby waves.

In addition, the jet core is also a maximum of the meridional gradient of absolute vorticity $\partial\overline{q}/\partial y$. As shown by Hoskins and Ambrizzi (1993), Rossby wave theory indicates that barotropic Rossby waves should refract toward this core maximum. As a consequence, Rossby waves that enter the NAA jet can become trapped and propagate along the length of the jet core, particularly as the flanks of the jet, which are minima of $\partial\overline{q}/\partial y$ (Fig. 2, bottom), act as refractive barriers and inhibit lateral escape from the jet.

4. Response to El Niño forcing

a. Response without sponge damping

We first present simulation anomaly composites for runs without sponge forcing. These results demonstrate the CAM4.0 undamped response to diabatic heating. Figure 3 shows the year-6–20 time-averaged differences of 200- and 500-hPa streamfunction for runs with El Niño diabatic forcing minus a run with no diabatic forcing. February El Niño diabatic forcing, applied to the area shown by the thick black outline, produces a
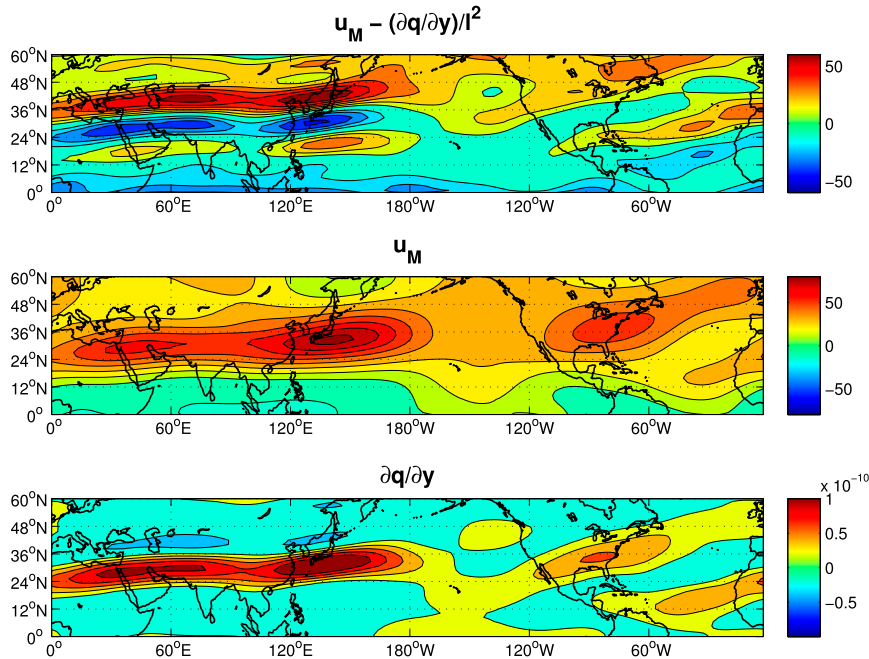
FIG. 2. Average (top) $u_M - [(\partial \overline{q}/\partial y)/l^2]$, (middle) u_M, and (bottom) $\partial \overline{q}/\partial y$ at 200 hPa for years 6–20 of a CAM4.0 perpetual February simulation performed without forcing or sponge relaxation. The average field has been zonally smoothed (wavenumbers 0–8). The contour interval is (top),(middle) $10\,\mathrm{m\,s}^{-1}$ and (bottom) $20 \times 10^{-11}\,(\mathrm{m\,s})^{-1}$.

large streamfunction response over the North Pacific. A wave train of alternating positive and negative anomalies extends northward from the forcing region in a pattern consistent with the PNA pattern (Wallace and Gutzler 1981). This pattern moves eastward over Alaska and northwestern Canada and then reflects southward over the continental United States.

The patterns at 200 and 500 hPa are similar over the North Pacific and North America, indicative of a barotropic wave structure; however, to the east over Africa and Asia, the extratropical response is more confined to the upper troposphere. A similar attenuation of an apparent eastward barotropic signal over the North Atlantic is seen in the meridional wind composite (Fig. 4). We will show in the next section that some of the signal over Asia is associated with westward-propagating waves in the NAA jet.

To examine further these eastward and westward waves, for the remainder of this study, we will focus on the upper-tropospheric response. Figure 5 shows the same El Niño composite for 200-hPa relative vorticity ζ, zonal wind, and velocity potential χ. The relative vorticity and zonal wind composites reveal anomalies over the North Pacific, which appear to reflect over western Canada and then propagate southeastward over the continental United States toward the Atlantic Ocean (the negative vorticity anomaly at 60°W east of Cuba

and the positive vorticity anomaly at 15°N, 30°W). This latter Rossby wave pattern has previously been described using ray tracing (Shaman and Tziperman 2005) and simulations with a linearized barotropic vorticity equation model (Shaman and Tziperman 2011; Shaman 2014). The pattern of alternating signed anomalies ceases over the subtropical North Atlantic at 15°N, 30°W where the entrance to the NAA jet lies (see Fig. 2). Within the jet itself the anomalies are single signed and consistent with a slowing, or even southward shift, of the jet winds.

El Niño forcing produces a pronounced pattern in the 200-hPa velocity potential anomaly field along the equator (Fig. 5, bottom). Negative anomalies, consistent with rising motion, are evident over much of the equatorial Pacific. Strong convergence and descent is also evident over the Indian Ocean and in part represents El Niño–forced changes to the Walker circulation.

b. Eastward-propagating waves

To isolate the eastward-propagating Rossby wave signal, we next applied damping from pole to pole and at all vertical levels to the west of the forcing region from 80° to 130°E in addition to El Niño forcing. The damping of westward-propagating wave activity clarifies the eastward-propagating Rossby wave signal in the streamfunction field (Fig. 6). The resolved wave train is
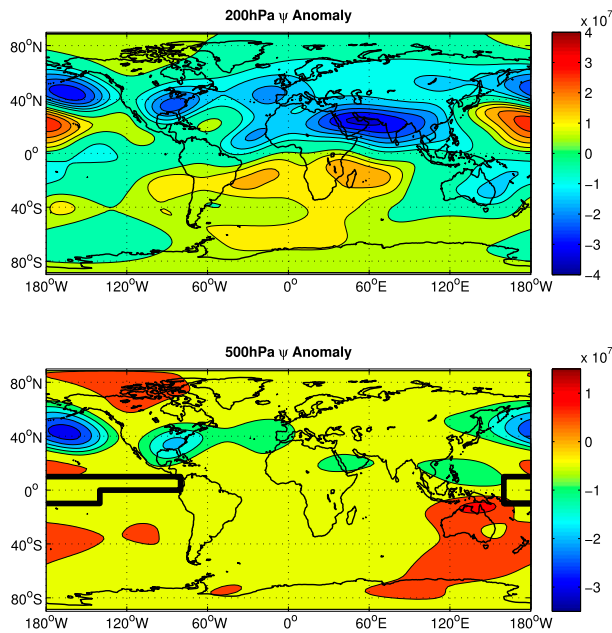
FIG. 3. February streamfunction anomalies associated with El Niño forcing. Shown are the average differences for years 6–20 at (top) 200 and (bottom) 500 hPa for a CAM4.0 simulation with El Niño diabatic forcing minus a CAM4.0 simulation with no forcing. The contour interval is 5×10^6 m^2 s^{-1}. The zero contour is omitted. The thick black line indicates the region of diabatic forcing.

FIG. 4. As in Fig. 3, but for meridional wind. The contour interval is 2 m s^{-1}. The zero contour is omitted.

now more clearly seen moving poleward and eastward over the North Pacific to western Canada and then moving southeastward to the tropical North Atlantic and the entrance of the NAA jet. Note specifically the part of the wave train indicated by positive anomalies over northernmost North America and just east of the Gulf of Mexico in Fig. 6, which are much weaker in the run with no sponge (Fig. 3).

Similar isolation of the eastward Rossby wave train can also be seen in the anomaly composites of the relative vorticity and zonal wind fields (Fig. 7). Indeed, these anomalies highlight a similar wave pattern that enters the NAA jet and remains trapped moving eastward to South Asia, just west of the damping region. The anomalies in the jet are consistent with a southward shift or slowing along the jet core just south of the Mediterranean Sea. The velocity potential response over the equatorial Indian Ocean is reduced but still substantial, indicating strong eastward propagation of anomalies along the equator in association with El Niño–forced changes to the Walker circulation.

c. Westward-propagating waves

We next performed the complementary experiment applying damping east of El Niño forcing from 60° to 10°W in order to isolate the westward-propagating Rossby wave signal. With this damping of the
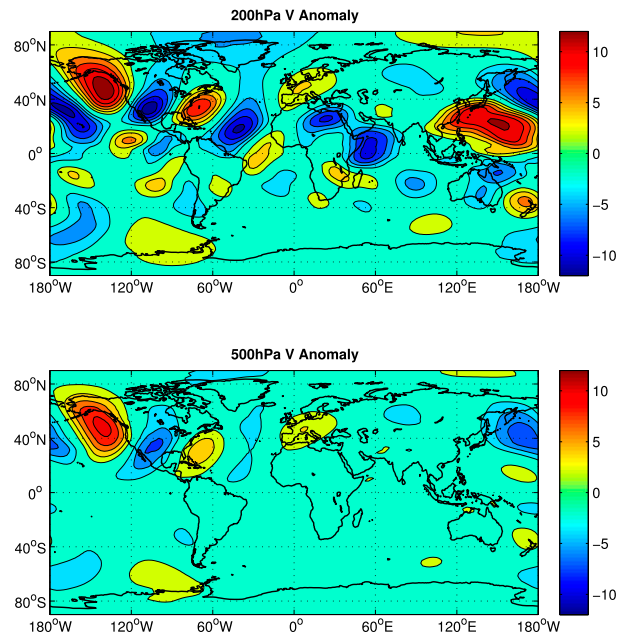
eastward wave signal, the westward upstream extension of single-signed streamfunction anomalies from the Pacific forcing region to Asia and Australia is evident (Fig. 8).

The response in the streamfunction field radiates outward and poleward from the Pacific forcing region; however, the relative vorticity and zonal wind composite anomalies are more horizontally constrained and align with the orientation of the NAA jet (Fig. 9). In particular, single-signed anomalies are again evident in the jet extending from East Asia to Africa, just east of the damping region. As for the eastward-propagating signal (Fig. 7), these anomalies are also indicative of a southward shift or slowing of the NAA jet core.

The location of the vorticity and zonal wind anomalies within the NAA jet is also collocated with the region in which $\overline{u}_M < (\partial \overline{q}/\partial y)/l^2$ (Fig. 2). This region should, in theory, support ultralow-wavenumber Rossby waves [Eq. (6)] that can travel rapidly westward and is consistent with the localized, single-signed response emanating westward from the North Pacific over southern Japan, China, and India.

The region of positive velocity potential anomalies over the Indian Ocean is more diminished with the sponge at 60°–10°W (Fig. 9) than with the sponge at 80°–130°E (Fig. 7). This finding again suggests eastward-propagating control of El Niño–forced velocity potential anomalies along the equator. There is also a new anomaly on the equator at the western edge of the
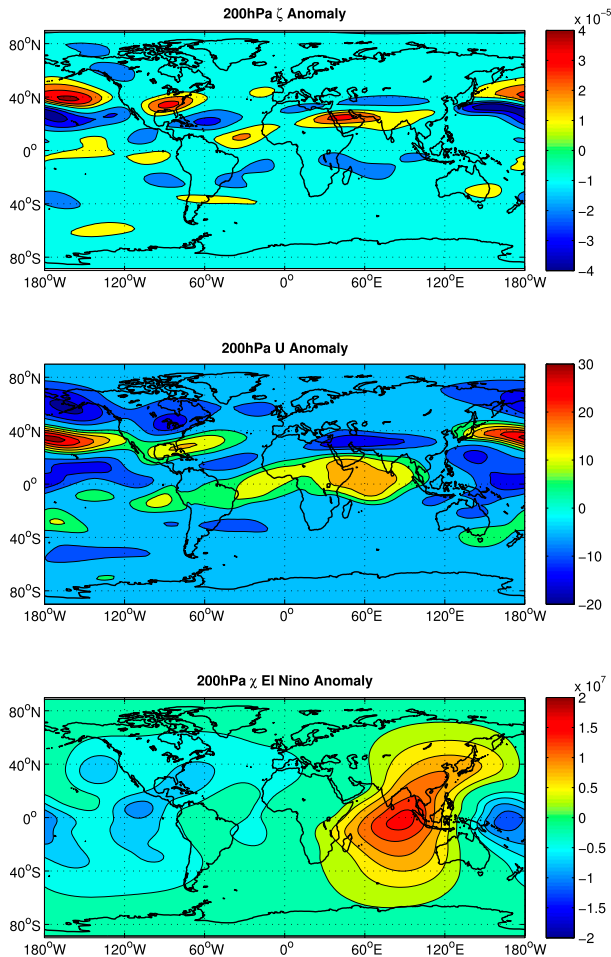
FIG. 5. As in Fig. 3 (top), but for composites of (top) ζ, (middle) zonal wind, and (bottom) χ. The contour intervals are $1 \times 10^{-6} \, \mathrm{s}^{-1}$, $5 \, \mathrm{m \, s}^{-1}$, and $2 \times 10^6 \, \mathrm{m}^2 \, \mathrm{s}^{-1}$, respectively. The zero contour is omitted in all instances.

FIG. 6. February streamfunction anomalies associated with El Niño forcing and damping at 80°–130°E. Shown are the average differences for years 6–20 at 200 hPa for a CAM4.0 simulation with El Niño diabatic forcing and sponge damping minus a CAM4.0 simulation with no forcing but the same sponge damping. The contour interval is $5 \times 10^6 \, \mathrm{m}^2 \, \mathrm{s}^{-1}$. The zero contour is omitted. Hatch marks delineate the sponge region.

sponge indicating an anomalous convergence of horizontal motion; this new anomaly is consistent with a slowing of El Niño–forced westerly wind anomalies as they encounter the sponge and a disruption of the anomalous Walker circulation.

d. Summing the signals

We next added the anomaly fields from the two damping experiments to determine whether a linear superposition of the eastward- and westward-propagating wave signals would reconstruct the undamped anomaly fields (i.e., Figs. 3 and 5) between the sponge regions away from El Niño diabatic forcing. The summed 200-hPa streamfunction anomalies (Fig. 10), in pattern, are remarkably consistent with the undamped anomalies to a degree that neither the eastward-propagating nor westward-propagating signals show (cf. Figs. 3 and 10 to Figs. 6 and 8). This
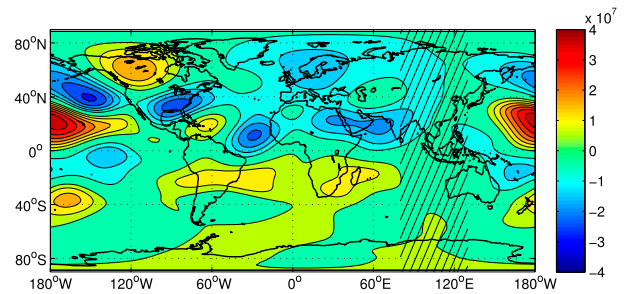
makes it clear that the remote response signal is a superposition of the two oppositely propagating signals. In particular, between the sponges in the area extending from the Indian subcontinent to northeastern Africa, between 10°W and 80°E, the summed streamfunction anomalies from the damped runs are similar in both spatial extent and magnitude to the undamped anomalies.

On the other hand, the relative vorticity and zonal wind summed anomalies (Fig. 11) reveal greater discrepancies from their undamped anomaly counterparts (Fig. 5). In particular, the magnitude of the response in NAA jet is greater in the summed vorticity and wind fields between the sponges over Asia. These findings indicate that the aggregate undamped response due to the competing eastward and westward waves (Fig. 5) is not wholly the result of a simple superposition of these signals but rather also includes some nonlinear interaction and possible negative feedback, which ultimately produces a more muted vorticity, and wind response over this region (Fig. 5).

5. Discussion

Here we have presented a new method for isolating the atmospheric response to waves propagating in different directions within an AGCM. We apply this at the planetary scale in the CAM4.0 AGCM and use it to isolate Rossby wave responses over Asia and Africa to boreal wintertime El Niño diabatic forcing. The new sponge methodology is shown to be capable of disentangling competing Rossby wave signals, and the findings indicate that both eastward- and westward-propagating Rossby wave activity is abundant in the atmosphere. Specifically our results show that El Niño generates waves propagating both east and west that
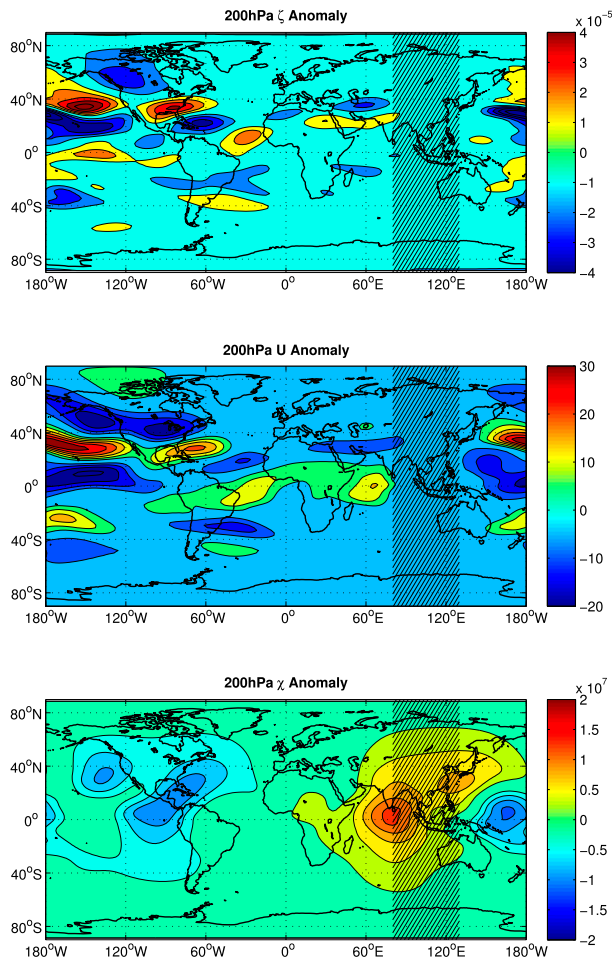
200hPa ζ Anomaly

200hPa U Anomaly

200hPa χ Anomaly

FIG. 7. As in Fig. 5, but for composites with damping applied at 80°–130°E. Hatch marks delineate the sponge region.

both contribute to the response in the North African–Asian (NAA) jet extending from the Indian subcontinent to northeastern Africa.

The location of the westward-propagating signal within the NAA jet is consistent with Rossby wave theory that describes the possibility of ultralow-wavenumber waves trapped in regions with strong meridional gradients of absolute vorticity. In such regions, which often coincide with jets, a single-signed anomaly response due to very long Rossby wave zonal wavelengths is expected and, in our CAM4.0 experiments, observed. These findings are consistent with prior work with a simpler model construct (Shaman et al. 2009).

Interestingly, the eastward-propagating Rossby wave response also produces a single-signed response in the NAA jet. It is not entirely clear why this occurs; however, the signal is more spatially intermittent. Indeed, the vorticity and zonal wind anomaly responses in the jet while single signed are not spatially continuous (Fig. 7). In particular, the negative vorticity anomalies are
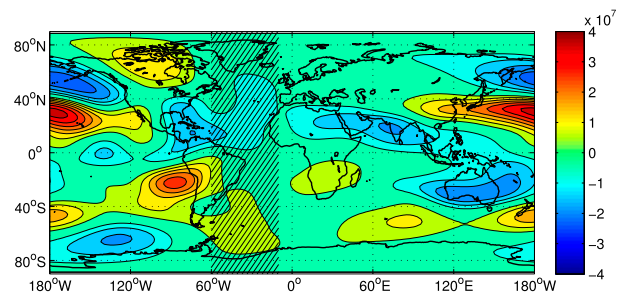

FIG. 8. As in Fig. 6, but for anomalies with damping at 60°–10°W.

present over North Africa and the Caspian Sea region but absent over the Mediterranean. Similarly, the wind anomalies are present west of Africa and over Arabia but missing over North Africa. These responses appear to be wavelike, albeit a wave that is biased to produce negative anomalies. It is possible that interactions within the jet produce this altered wave structure. In contrast, the westward response, which we suspect is due to
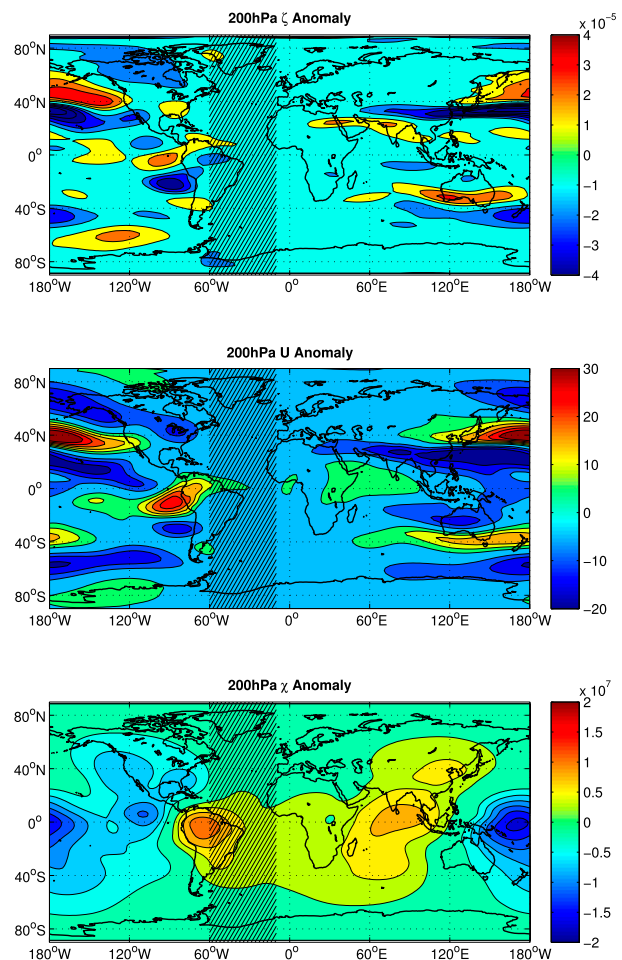

200hPa ζ Anomaly

200hPa U Anomaly

200hPa χ Anomaly

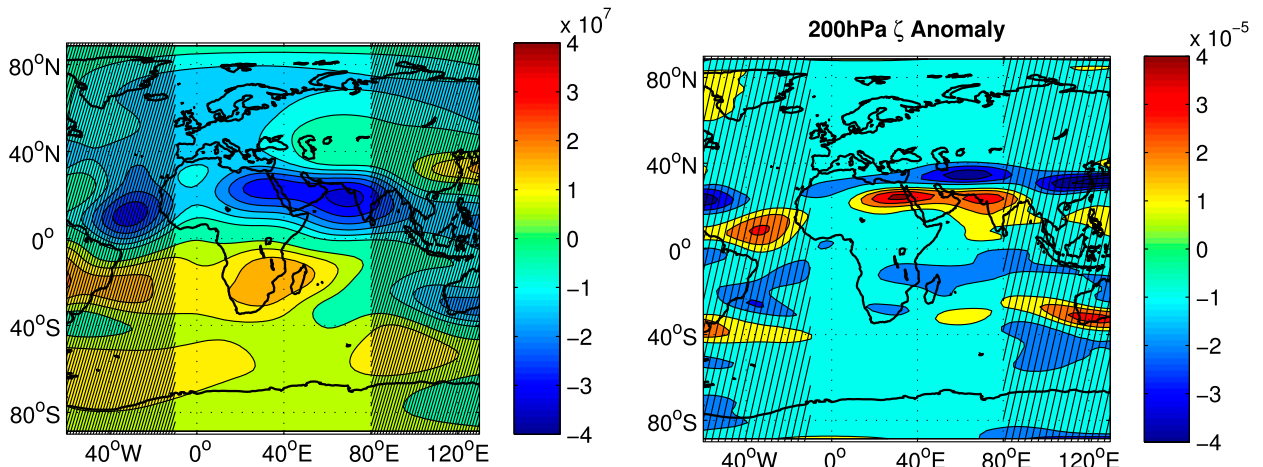FIG. 9. As in Fig. 7, but for composites with damping applied at 60°–10°W.

FIG. 10. Summation of the streamfunction anomaly fields displayed in Figs. 6 and 8. The contour interval is $5 \times 10^6 \, \mathrm{m^2 \, s^{-1}}$. The zero contour is omitted. Hatch marks delineate the two sponge regions.

ultralow-wavenumber Rossby waves, is continuous and strong and shows no suggestion of an alternately signed wave structure (Fig. 9).

The aggregate response in the NAA jet, while mostly linear, appears to be more than a simple superposition of the eastward- and westward-propagating signals. Indeed, for the relative vorticity and zonal wind fields, the undamped upper-tropospheric response is muted (Fig. 5) relative to the summed response of the two individual signals (Fig. 11). Similarly, the summed positive velocity potential anomalies south of India (Fig. 11, bottom) are stronger than the anomalies in the undamped composite (Fig. 5, bottom), suggesting some nonlinear damping of the Rossby wave source associated with that remote convergence. These findings suggest that some form of interaction—wave–mean flow, wave–wave interference, moist processes, and so forth—acts to negatively feed back on the component waves.

We additionally explored whether El Niño diabatic forcing and the sponge produce any downstream, nonlinear effects, including the generation of waves in remote locations. To test this, we repeated our experiments with the diabatic forcing strength halved. These simulations (not shown) produced anomaly patterns with similar spatial structure and about half the magnitude of the full forcing experiments (Figs. 6–11). We therefore conclude that the overall response to El Niño forcing is primarily linear, even in the presence of the sponge. There is some evidence of a sponge-induced change to the anomalous Walker circulation in response to El Niño diabatic heating (see Fig. 9, the velocity potential anomalies); however, this change does not
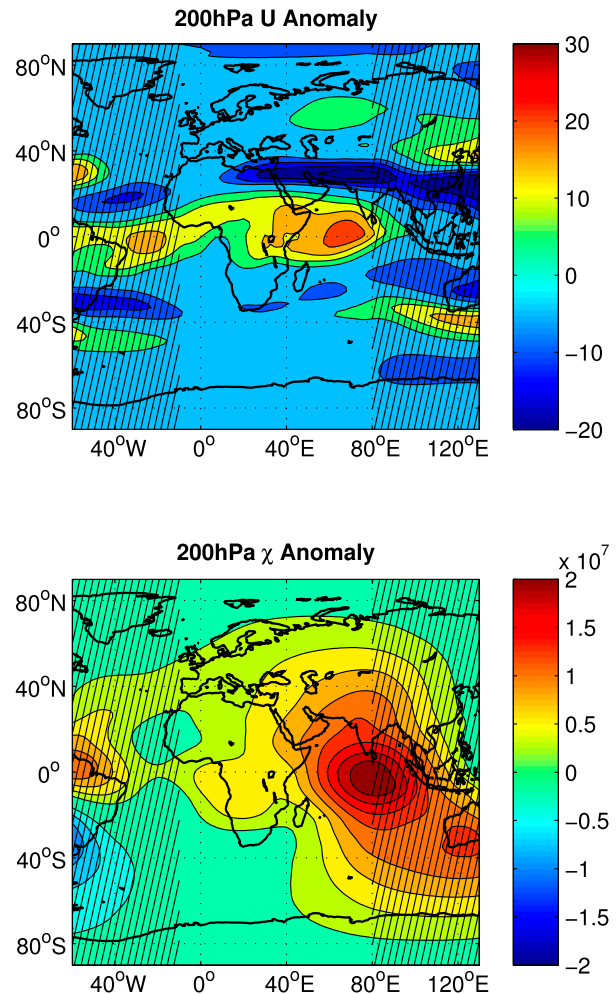

FIG. 11. Summation of ζ, zonal wind and χ anomaly fields displayed in Figs. 7 and 9. The contour intervals are (top) $1 \times 10^{-6} \, \mathrm{s^{-1}}$, (middle) $5 \, \mathrm{m \, s^{-1}}$, and (bottom) $2 \times 10^6 \, \mathrm{m^2 \, s^{-1}}$. The zero contour is omitted in all instances. Hatch marks delineate the two sponge regions.

appear to produce further excitation of Rossby waves as indicated by the overall linearity of the response to El Niño diabatic forcing.

Use of a time-evolving AGCM to examine the response to tropical heating affords representation of many atmospheric processes that more idealized models do not depict. In particular, transient effects, including downstream diabatic heating and transient forcing due to heat and vorticity flux convergence (e.g., Ting and Hoerling 1993), as well as nonlinear processes, such as wave–wave and wave–mean flow interactions, are simulated. Such processes have been shown to be important for downstream modification of planetary waves (Held and Kang 1987; Held et al. 1989; Hoerling and Ting 1994; Trenberth et al. 1998) and cannot be represented explicitly by more primitive steady-state or linearized models.

It should be noted that simple linearized models can capture much of the NAA jet response to El Niño forcing (e.g., Shaman 2014); however, for the purposes of this study, in which we explicitly disentangled eastward- and westward-propagating Rossby wave signals, it was important to employ a detailed time-evolving fully nonlinear AGCM to determine whether nonlinear interactions occur between these competing wave signals. The findings from this study indicate that within the NAA jet, the combined response is mostly a linear superposition of the two wave signals with some additional weaker nonlinear effects. Further, both the eastward- and westward-propagating waves appear to be trapped in the NAA jet, consistent with Rossby wave theory (Hoskins and Ambrizzi 1993), which predicts wave refraction toward the maximum of the meridional gradient of potential vorticity that extends along the core of the jet.

In the future, we plan to apply this sponge methodology to the study of other systems and track the origins of wave activity with greater precision. In doing so, we hope to explore the sources of remote response within the atmosphere, as represented by an AGCM.

REFERENCES

Barlow, M., A. Hoell, and F. Colby, 2007: Examining the wintertime response to tropical convection over the eastern Indian Ocean by modifying atmospheric heating in a global atmospheric model. *Geophys. Res. Lett.*, **34**, L19702, doi:10.1029/2007GL030043.

Bender, C. M., and S. A. Orszag, 1978: *Advanced Mathematical Methods for Scientists and Engineers.* McGraw-Hill, 593 pp.

Branstator, G., 1985: Analysis of general circulation model sea-surface temperature anomaly simulations using a linear model. Part II: Eigenanalysis. *J. Atmos. Sci.*, **42**, 2242–2254, doi:10.1175/1520-0469(1985)042<2242:AOGCMS>2.0.CO;2.

Held, I. M., and I.-S. Kang, 1987: Barotropic models of the extratropical response to El Niño. *J. Atmos. Sci.*, **44**, 3576–3586, doi:10.1175/1520-0469(1987)044<3576:BMOTER>2.0.CO;2.

——, S. W. Lyons, and S. Nigam, 1989: Transients and the extratropical response to El Niño. *J. Atmos. Sci.*, **46**, 163–174, doi:10.1175/1520-0469(1989)046<0163:TATERT>2.0.CO;2.

Hoerling, M. P., and M.-F. Ting, 1994: Organization of extratropical transients during El Niño. *J. Climate*, **7**, 745–766, doi:10.1175/1520-0442(1994)007<0745:OOETDE>2.0.CO;2.

Hoskins, B. J., and K. Karoly, 1981: The steady response of a spherical atmosphere to thermal and orographic forcing. *J. Atmos. Sci.*, **38**, 1179–1196, doi:10.1175/1520-0469(1981)038<1179:TSLROA>2.0.CO;2.

——, and T. Ambrizzi, 1993: Rossby wave propagation on a realistic longitudinally varying flow. *J. Atmos. Sci.*, **50**, 1661–1671, doi:10.1175/1520-0469(1993)050<1661:RWPOAR>2.0.CO;2.

Hurrell, J. W., J. J. Hack, D. Shea, J. M. Caron, and J. Rosinski, 2008: A new sea surface temperature and sea ice boundary dataset for the Community Atmospheric Model. *J. Climate*, **21**, 5145–5153, doi:10.1175/2008JCLI2292.1.

Karoly, D., 1983: Rossby wave propagation in a barotropic atmosphere. *Dyn. Atmos. Oceans*, **7**, 111–125, doi:10.1016/0377-0265(83)90013-1.

Kucharski, F., A. Bracco, J. Yoo, A. Tompkins, L. Feudale, P. Ruti, and A. Dell'Aquila, 2009: A Gill–Matsuno-type mechanism explains the tropical Atlantic influence on African and Indian monsoon rainfall. *Quart. J. Roy. Meteor. Soc.*, **135**, 569–579, doi:10.1002/qj.406.

Li, Z., and T. R. Nathan, 1997: Effects of low-frequency tropical forcing on intraseasonal tropical–extratropical interactions. *J. Atmos. Sci.*, **54**, 332–346, doi:10.1175/1520-0469(1997)054<0332:EOLFTF>2.0.CO;2.

Neale, R. B., and Coauthors, 2010: Description of the NCAR Community Climate Model (CAM 4.0). NCAR Tech. Note TN-485+STR, 224 pp.

Nigam, S., and E. DeWeaver, 1998: Influence of orography on the extratropical response to El Niño event. *J. Climate*, **11**, 716–733, doi:10.1175/1520-0442(1998)011<0716:IOOOTE>2.0.CO;2.

Rossby, C. G., 1939: Relation between variations in the intensity of the zonal circulation of the atmosphere and the displacements of the semi-permanent centers of action. *J. Mar. Res.*, **2**, 38–55, doi:10.1357/002224039806649023.

Shaman, J., 2014: The seasonal effects of ENSO on atmospheric conditions associated with European precipitation: Model simulations of seasonal teleconnections. *J. Climate*, **27**, 1010–1028, doi:10.1175/JCLI-D-12-00734.1.

——, and E. Tziperman, 2005: The effect of ENSO on Tibetan Plateau snow depth: A stationary wave teleconnection mechanism and implications for the South Asian monsoons. *J. Climate*, **18**, 2067–2079, doi:10.1175/JCLI3391.1.

——, and ——, 2011: An atmospheric teleconnection linking ENSO and southwestern European precipitation. *J. Climate*, **24**, 124–139, doi:10.1175/2010JCLI3590.1.

——, S. K. Esbensen, and E. D. Maloney, 2009: The dynamics of the ENSO–Atlantic hurricane teleconnection: ENSO-related changes to the North African–Asian jet affect Atlantic basin tropical cyclogenesis. *J. Climate*, **22**, 2458–2482, doi:10.1175/2008JCLI2360.1.

——, R. Samelson, and E. Tziperman, 2012: Complex wavenumber Rossby wave ray tracing. *J. Atmos. Sci.*, **69**, 2112–2133, doi:10.1175/JAS-D-11-0193.1.

Simmons, A. J., J. M. Wallace, and G. W. Branstator, 1983: Barotropic wave propagation and instability, and atmospheric teleconnection patterns. *J. Atmos. Sci.*, **40**, 1363–1392, doi:10.1175/1520-0469(1983)040<1363:BWPAIA>2.0.CO;2.

Sobel, A. H., and C. S. Bretherton, 1999: Development of synoptic-scale disturbance over the summertime tropical northwest Pacific. *J. Atmos. Sci.*, **56**, 3106–3127, doi:10.1175/1520-0469(1999)056<3106:DOSSDO>2.0.CO;2.

Ting, M.-F., and M. P. Hoerling, 1993: Dynamics of stationary wave anomalies during the 1986/87 El Niño. *Climate Dyn.*, **9**, 147–164, doi:10.1007/BF00209751.

Trenberth, K. E., G. W. Branstator, D. Karoly, A. Kumar, N.-C. Lau, and C. Ropelewski, 1998: Progress during TOGA in understanding and modeling global teleconnections associated with tropical sea surface temperatures. *J. Geophys. Res.*, **103**, 14 291–14 324, doi:10.1029/97JC01444.

Wallace, J. M., and D. S. Gutzler, 1981: Teleconnections in the geopotential height field during the Northern Hemisphere winter. *Mon. Wea. Rev.*, **109**, 784–811, doi:10.1175/1520-0493(1981)109<0784:TITGHF>2.0.CO;2.

Wang, Y., K. Yamazaki, and Y. Fujiyoshi, 2007: The interaction between two separate propagations of Rossby waves. *Mon. Wea. Rev.*, **135**, 3521–3540, doi:10.1175/MWR3486.1.